Monolithically integrated widely tunable laser source operating at 2 μm

Latkowski, S; Hänsel, A.; Van Veldhoven, P. J.; D'Agostino, D.; Rabbani-Haghighi, H.; Docter, B.; Bhattacharya, N.; Thijs, P. J A; Ambrosius, H. P M M; Smit, M. K.

DOI
10.1364/OPTICA.3.001412

Publication date
2016

Document Version
Final published version

Published in
Optica

Research Article Vol. 3, No. 12 / December 2016 / Optica 1412

Monolithically integrated widely tunable laser source operating at 2 μm

S. Latkowski,[1,*] A. Hänsel,[2] P. J. van Veldhoven,[1] D. D'Agostino,[1] H. Rabbani-Haghighi,[1] B. Docter,[3] N. Bhattacharya,[2] P. J. A. Thijs,[1] H. P. M. M. Ambrosius,[1] M. K. Smit,[1] K. A. Williams,[1] and E. A. J. M. Bente[1]

[1]COBRA Research Institute, Eindhoven University of Technology, De Rondom 70, 5612 AP, Eindhoven, The Netherlands
[2]Optics Research Group, TU Delft, Lorentzweg 1, 2628 CJ, Delft, The Netherlands
[3]EFFECT Photonics B.V., Torenallee 20, 5617 BC, Eindhoven, The Netherlands
*Corresponding author: S.Latkowski@tue.nl

Received 8 July 2016; revised 30 September 2016; accepted 4 October 2016 (Doc. ID 270075); published 21 November 2016

We present a widely tunable extended cavity ring laser operating at 2 μm that is monolithically integrated on an indium phosphide substrate. The photonic integrated circuit is designed and fabricated within a multiproject wafer run using a generic integration technology platform. The laser features an intracavity tuning mechanism based on nested asymmetric Mach–Zehnder interferometers with voltage controlled electro-refractive modulators. The laser operates in a single-mode regime and is tunable over the recorded wavelength range of 31 nm, spanning from 2011 to 2042 nm. Its capability for high-resolution scanning is demonstrated in a single-line spectroscopy experiment using a carbon dioxide reference cell.

OCIS codes: (250.5960) Semiconductor lasers; (140.3600) Lasers, tunable; (250.5300) Photonic integrated circuits; (300.0300) Spectroscopy; (280.3420) Laser sensors.

http://dx.doi.org/10.1364/OPTICA.3.001412

1. INTRODUCTION

Generic photonic integration technology platforms provide application oriented specialists with the means of designing affordable application-specific photonic integrated circuits (ASPIC) [1]. In such technology platforms a limited set of functionalities for on-chip manipulation of light are predefined in a form of building blocks (BB). These BBs are used to design photonic integrated circuits (PICs) of complex topologies in order to realize application-oriented functions. An important factor defining the scope of potential applications for these ASPICs is the range of accessible wavelengths. The ASPICs operating in the mid-infrared wavelengths range beyond 2 μm are particularly interesting for the applications in gas spectroscopy [2]. This is related to the presence of absorption profiles of several gas species, for example, acetone, ammonia, carbon dioxide, water vapor, formaldehyde, diethylamine, ethylamine, and methylamine [3]. A trace analysis of such gas species is important in a wide range of applications including environmental monitoring in agriculture, process control in chemical and pharmaceutical plants and laboratories, atmospheric pollution monitoring, and for medical monitoring and diagnosis. Furthermore, the use of a monolithic photonic integration technology allows for the co-integration of several sources and detection subsystems on a single chip making it particularly attractive for multispecies gas detection systems where the complexity and size of bulk optics-based solutions are in many cases prohibitive factors [2,4].

Record results [5–10] in terms of output power and efficiency were achieved at the long wavelength range at 2 μm and beyond with the use of various material systems and quantum well configurations. Both monolithic [11] and heterogeneous integration [12] technologies that enable access to wavelength bands in the range from 2 to 10 μm have also been demonstrated. These approaches, although setting the state-of-the-art in terms of reported performance, are based on highly customized processes and frequently require the addition of new materials. The long wavelength integration technology platform presented in this paper is almost identical to the standard technology process used for the fabrication of PICs and devices at 1.5 μm and can be seamlessly transferred to a foundry having such processes in place.

It has been demonstrated that the wavelengths around 2 μm can be generated and amplified using indium phosphide (InP)-based strained InGaAs quantum well and quantum dash-based material systems [13–15]. An extended wavelength range of an InP active–passive photonic integration technology platform has been demonstrated in our COBRA research institute up to 1.75 μm, targeting applications in optical coherence tomography [16]. Further development of the capabilities of this integration platform toward longer wavelengths was based on strained quantum wells [17]. These efforts allowed for the first successful fabrication of a full multiproject wafer (MPW) run with optical amplifiers operating at wavelengths beyond 2 μm [1,18,19]. In this MPW, a tunable laser operating at such long wavelengths

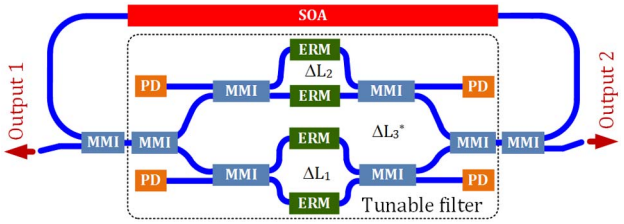

Fig. 1. Schematic diagram of the PIC-based tunable ring laser with an intracavity wavelength-tunable filter (in a dashed box) based on a nested asymmetric Mach–Zehnder interferometer. The PIC consists of the following building blocks connected by passive waveguides (in blue): SOA, a semiconductor optical amplifier; MMI, multimode interference couplers; ERM, electro-refractive modulators; and PD, photodiodes. The light is coupled out from the laser cavity with two MMIs.

was realized as a monolithic InP-based PIC. The circuit layout of this laser is depicted schematically in Fig. 1. Following the generic integration approach, the laser cavity is designed using a predefined set of basic BBs [1,20]. These BBs are the semiconductor optical amplifier (SOA), electro-refractive modulator (ERM), and passive waveguide based devices such as splitters and waveguides. The wavelength tuning is achieved with an intracavity filter based on nested asymmetric Mach–Zehnder interferometers (AMZI) with ERMs as tuning elements [19,21–23]. This ensures that the laser operates in a single longitudinal mode and in combination with the gain bandwidth of the strained quantum well-based SOAs it achieves a tuning range of 31 nm. To our knowledge, such a tuning range exceeds those provided by other monolithic semiconductor devices reported in literature [6,14,15,24,25], be it PICs realized in monolithic [18,19] or hybrid technologies [4,26].

2. MONOLITHIC PIC

A. Active-Passive Integration

In the generic active-passive photonic integration technology developed in the COBRA research institute all BBs are realized on one of the two types of epitaxial layer stacks: active or passive. Both are grown on the same indium phosphide substrate [1]. In order to change the accessible wavelength range of the available InP integration technology at 1.5 μm to the wavelengths beyond 2 μm a number of changes in the vertical layer-stack (Table 1) were introduced [27] and are discussed in the following paragraphs of this section. The processing steps in such a long wavelength technology are nearly the same as those of 1.5 μm InP technology.

The main contribution to the propagation loss in the passive waveguides is attributed to the absorption in p-doped layers grown on top of the undoped quaternary (InGaAsP) waveguiding core, as presented in Table 1. In order to reduce the propagation loss resulting from an overlap of the optical mode with highly doped cladding layers the thickness of the waveguiding core was increased from 500 nm used in the standard 1.5 μm COBRA technology to 625 nm in the long wavelength platform.

The optically active waveguide features a centrally located active core based on a multiple quantum well (MQW) structure with compressively strained (1.75%) $In_{1-x}Ga_xAs$ quantum wells (QW) with a gallium fraction of 0.22. The strained QW layers were grown at a low temperature (560°C) in a metalorganic vapor phase epitaxy (MOVPE) reactor. In contrast to earlier published

Table 1. Epitaxial Layer Stack and Top Metallization Layers of Active and Passive Waveguides

Thickness	Active	Passive
600 nm	Au	
150 nm	Ti/Pt/Au	
300 nm	InGaAs ($1.5 * 10^{19}$ cm^{-3} P)	
1000 nm	InP (10^{18} cm^{-3} P)	
500 nm	InP (10^{17} cm^{-3} P)	
	Wave-guiding core—625 nm	
218.0 nm	$In_{0.74}Ga_{0.26}As_{0.57}P_{0.43}$	
37.5 nm	$In_{0.53}Ga_{0.47}As$	
6.0 nm	$In_{0.78}Ga_{0.22}As$ strained QW	
30.0 nm	$In_{0.53}Ga_{0.47}As$	
6.0 nm	$In_{0.78}Ga_{0.22}As$ strained QW	
30.0 nm	$In_{0.53}Ga_{0.47}As$	$In_{0.74}Ga_{0.26}As_{0.57}P_{0.43}$
6.0 nm	$In_{0.78}Ga_{0.22}As$ strained QW	
30.0 nm	$In_{0.53}Ga_{0.47}As$	
6.0 nm	$In_{0.78}Ga_{0.22}As$ strained QW	
37.5 nm	$In_{0.53}Ga_{0.47}As$	
218.0 nm	$In_{0.74}Ga_{0.26}As_{0.57}P_{0.43}$	
70.0 nm	InP (undoped)	
430.0 nm	InP ($5.0 * 10^{17}$ cm^{-3}N)	
300 μm	InP (substrate)	

work regarding the development of the gain stack [14,17,28] no antimony (Sb) was added as a surfactant.

Two types of ridge waveguide (RWG) structures are used in the long wavelength COBRA active-passive technology. Shallow waveguides feature a 2.5 μm wide ridge and are etched 100 nm into the waveguiding quaternary layer. The deep waveguides are 2 μm wide and are etched 150 nm into the bottom InP cladding layers. Passive waveguides and the ERMs use a quaternary material ($In_{0.74}Ga_{0.26}As_{0.57}P_{0.43}$)-based 625 nm thick waveguiding layer with propagation losses of 8 dB/cm. The optically active BBs, the semiconductor optical amplifier and the photodiode, feature the strained MQW active core and are realized as shallow type RWGs. Net modal gain of a RWG SOA was measured using a multisection device method [29]. A spectrum of the net modal gain measured at a current density of 3.6 kA/cm^2 and a temperature set at 17°C is shown in Fig. 2.

In addition to the passive waveguides and semiconductor optical amplifiers, other functions were implemented based on these two types of the active and passive layer stacks in order to complete the long wavelength technology platform. MMIs providing means of splitting and combining the light, ERMs for manipulating the phase of the optical signals, and on-chip photodetectors were defined in order to provide a basic set of BBs. These BBs allow the realization of a complex laser cavity in the form of monolithic PIC.

B. Widely Tunable Laser

A novel geometry widely tunable laser was developed taking into account constraints imposed by generic integration technology. A ring laser featuring an intracavity wavelength tunable filter based on asymmetric Mach–Zehnder interferometers [22] in a nested configuration [19,23], as shown in Fig. 1, was designed in the form of a PIC, as presented in Fig. 3.

Performance of the predefined BBs available in the long wavelength active-passive technology had to be accounted for in the design process of the laser. In particular, the available gain and its

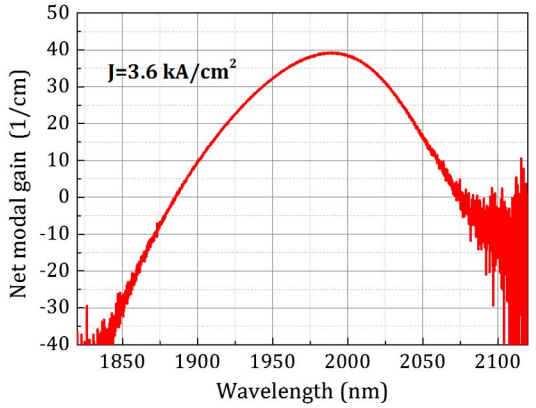

Fig. 2. Net modal gain of a long wavelength ridge waveguide semiconductor optical amplifier, based on the strained multiple quantum well material, measured using the segmented contact method at current density J = 3.6 kA/cm^2 and a temperature of 17°C.

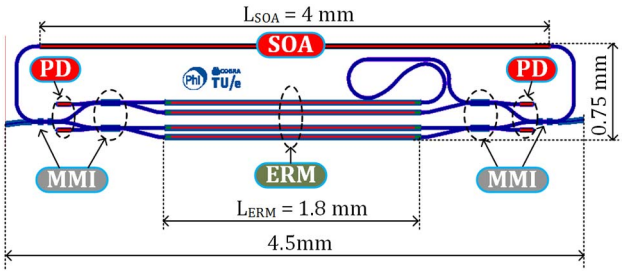

Fig. 3. Mask layout of the ring laser with a nested AMZI intracavity filter. The laser features a 4 mm long SOA and a four branch AMZI filter with 1.8 mm long ERMs for wavelength tuning. The multimode interference couplers (MMI) and deep etched passive waveguides are used to form the AMZI filter and couple the light out of the cavity. The ring cavity is closed by deep etched passive waveguides. The output waveguides are angled with respect to the chip facets (7° to the normal) in order to reduce reflections. The laser occupies an area of 3.4 mm^2.

bandwidth, propagation losses in passive waveguides, and efficiency of the phase shifters. These parameters have a direct impact on the overall cavity length and the resulting cavity mode spacing. The cavity mode spacing in combination with the gain profile of the amplifier impose requirements on the free spectral range and selectivity of the intracavity filter in order to assure a single-mode operation over a wide range of wavelengths [22,30].

The two internal AMZI stages featuring physical path length imbalances of $\Delta L_1 = 2110$ μm and $\Delta L_2 = 16$ μm are nested in a third one with a path length imbalance of $\Delta L_3^* = 74$ μm. The imbalance ΔL_3^* introduced in the outer AMZI results in an interferometric filter in which there are six path length differences in parallel. Each AMZI stage features a periodic transmission with respect to frequency with a free spectral range of $FSR_N = v_g(f)/\Delta L_N$ with $v_g(f)$ being the frequency-dependent group velocity. The ring cavity with this nested AMZI filter has an average physical length of 9 mm resulting in a free spectral range (FSR) of ~9 GHz. The imbalances in all stages of the AMZI filter are chosen in such a way that one longitudinal mode can be selected within the gain bandwidth of the amplifier. The other modes within the gain bandwidth experience a sufficient loss

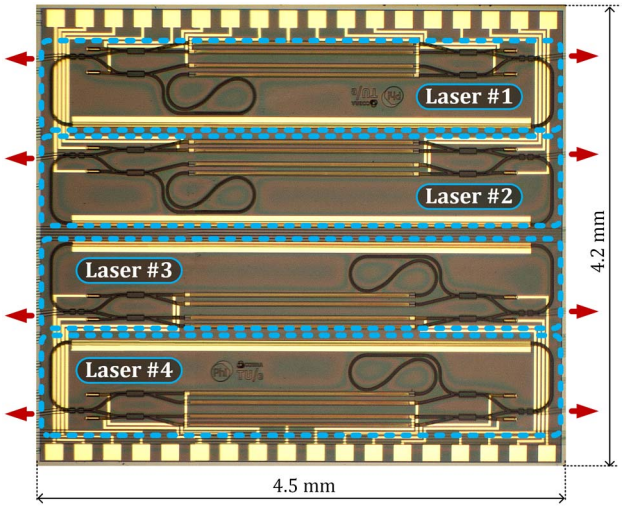

Fig. 4. Microscope image of a 19 mm^2 ASPIC. The chip was fabricated in a MPW run using COBRA long wavelength active-passive integration technology. The ASPIC includes four widely tunable lasers (blue dashed boxes) and occupies a single standard MPW cell.

in comparison to the selected mode. This allows for single-mode operation of the laser [30]. The optical gain is provided by a 4 mm long and 2.5 μm wide SOA. The AMZI stages in the wavelength tunable filter inside the laser cavity are formed by passive waveguides and MMIs with 1.8 mm long ERM ($V_{2\pi} = 23$ V) sections added in each branch in order to enable its tuning by applying reverse bias voltages as control signals. Two inner AMZI stages of the filter have PDs added on both sides of each stage for on-chip monitoring and calibration functionalities. The ring cavity is closed with deep passive waveguides (propagation loss of 8 dB/cm [18]) and the signals are coupled out from the laser with two 1 × 2 MMI elements. The light is routed to the output ports, which are angled with respect to the cleaved edges of the chip to reduce reflections. The resulting mask layout of one device occupies an area of 3.4 mm^2, as shown in Fig. 3. A 19 mm^2 chip including four such lasers was fabricated within a MPW run at the NanoLab@TU/e cleanroom. A microscope micrograph of the fabricated chip is shown in Fig. 4. Additional functions can be implemented into such monolithic chips. For example, the lasers can be combined into a single-output waveguide as, was demonstrated with 1.5 μm technology [31].

The wavelength tunability is achieved by means of the optical phase changes introduced in each branch of the nested AMZI filter and can be realized by applying control signals continuously and simultaneously to all of the ERM sections. Such continuous tuning of the AMZI laser over a wide wavelength range should be realizable in practice, provided that the refractive index change in the ERM as a function of the control voltage and wavelength is known. Furthermore, all of the control signals should be applied in a timely manner and the changes at 2π phase points should be executed sufficiently fast, i.e., below the onset time of the laser (typically on the order of a few nanoseconds). In addition to the tuning with the ERM sections the laser can be tuned over a limited frequency range (on the order of its free spectral range) with a single control signal being the current injected into the SOA element or the temperature of the device.

3. EXPERIMENTAL RESULTS

The fabricated chip is mounted on an aluminum block and all electrical contacts are wire bonded to a signal distribution printed circuit board. The submount is temperature stabilized with a passive water cooling system at 18°C. The optical signal is collected with an antireflection coated, lensed, single-mode fiber (coupling loss of ~5 dB) and fed via an optical isolator to the measurement equipment. An amplified extended InGaAs photodiode (Thorlabs PDA10D) was used to record the total optical output power coupled into the fiber as a function of bias current injected into the SOA section. The measured optical power was calibrated using a responsivity curve of the PD and the gain parameters of the amplifier and cross-compared with the power measurements obtained with an optical spectrum analyzer. The collected output power and voltage drop across the SOA section with respect to the injected current into the SOA section (LVI) characteristic was recorded with all ERMs grounded and is presented in Fig. 5. It shows the lasing threshold point to be at 360 mA (3.6 kA/cm^2), with a maximum fiber coupled power of 95 μW, assuming a 5 dB chip to fiber coupling power loss of ~0.3 mW ex-facet. Assuming most of the resistance visible in the VI curve of the laser is in the SOA contact, a contact resistivity of $5.4 \cdot 10^{-8}\ \Omega \cdot m^2$ was determined. The LI curve was measured with the ERM sections biased at 0 V, as the three AMZI filters were not aligned; changes in the lasing mode can be observed at currents in the vicinity of 400 mA. Compared to devices fabricated using standard 1.5 μm technology the wall-plug efficiency is low. This is attributed to higher roundtrip losses and the amplifier. The passive elements in the cavity at 2 μm have approximately twice the loss per unit length compared to the components at 1.5 μm. The optical losses in the amplifier are assumed to be considerably higher, which is reflected in a reduced modal gain compared to 1.5 μm amplifiers. Furthermore, the light is coupled out from the laser after the tuning filter, which favors the spectral quality over the output power. A Yokogawa AQ6375 optical spectrum analyzer with a 0.05 nm resolution was used to record the optical spectra for several different sets of reverse bias voltages applied to the ERM sections, with the SOA current and temperature of the heatsink being constant at $I_{SOA} = 450$ mA and $T_{HS} = 18$°C, respectively. These spectra are overlapped and presented in Fig. 6. The laser output covers an over 31 nm wide tuning range centered at 2027 nm. The device provides a single longitudinal-mode output with a side mode suppression ratio (SMSR) of more than 30 dB at each measured operating point across the whole tuning range.

In order to verify the accuracy of the tuning mechanism and the laser's suitability for use in the gas sensing environment, it was employed in a basic gas spectroscopy setup. The output from the laser was split in half using a fiberized optical coupler provided with a probe and reference signals. The reference signal was directed onto a PD (Ultrafast Sensors FIR083) in order to monitor any intensity fluctuations and the probe signal was collimated into the free space beam and sent through a CO_2 gas cell followed by another PD (Thorlabs PDA10). The gas interaction region was a 100 mm long cylindrical reference cell (Precision Glassblowing TG – ABCO$_2$ – Q) with 19 mm diameter and angled (2°) windows, filled with the CO_2 at a pressure of 76 Torr (0.1 atm). The laser output was tuned by using the ERMs to target a particular absorption line and sweep over it by applying changes of the injection current into the SOA section. A change of the SOA current from 420 to 490 mA, in steps of 0.25 mA, resulted in a wavelength tuning of 14 GHz with a frequency step of 50 MHz ($\Delta\lambda \sim 676$ fm). Such a tuning range is wider than the cavity mode spacing of the laser. A measurement of the strongest CO_2 absorption line within the laser tuning range is presented (blue circles) in Fig. 7. Its spectral width of 864 MHz and maximum absorption of 56% shows a very good agreement with the simulated spectrum (red line). The measured data is overlapped with a simulated profile of the CO_2 absorption using the HITRAN database and online tool [32,33], with the input parameters corresponding to the reference gas cell. The frequency scale over the tuning range was calibrated using the Yokogawa optical spectrum analyzer. The inset in Fig. 7 presents the measured absorption spectra of four more CO_2 transitions as well as the transition in the main graph. For each absorption line, the laser was tuned using the voltage settings on the ERMs and scanned over the line using the same current sweep.

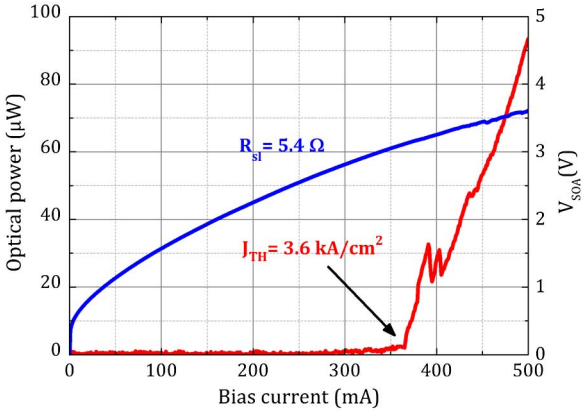

Fig. 5. LVI characteristics. The fiber-coupled average optical power as a function of the SOA current (in red) shows a threshold current $I_{TH} = 360$ mA (current density $J_{TH} = 3.6$ kA/cm^2), and a maximum power of 97 μW, which corresponds to 0.3 mW of ex-facet power (assuming a chip to fiber coupling loss of 5 dB). The voltage drop across the SOA against the injected current (in blue) indicates a slope resistance of 5.4 Ω or a contact resistance of $5.4 \cdot 10^{-8}\ \Omega \cdot m^2$.

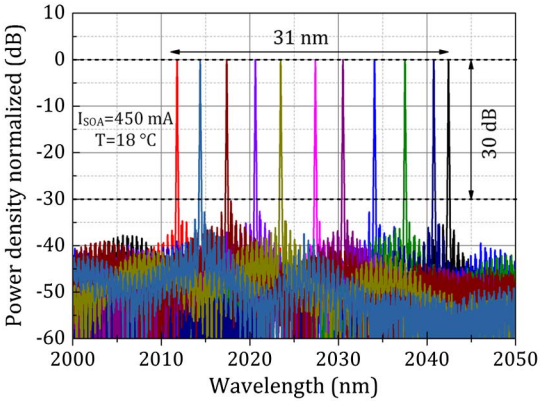

Fig. 6. Optical spectra recorded using an optical spectrum analyzer for different sets of reverse bias voltages applied to the ERM sections while both the injection current into the SOA section and the temperature were kept constant at $I_{SOA} = 450$ mA and $T_{HS} = 18$°C, respectively. At such tuning conditions the laser covers a record tuning range of 31 nm.

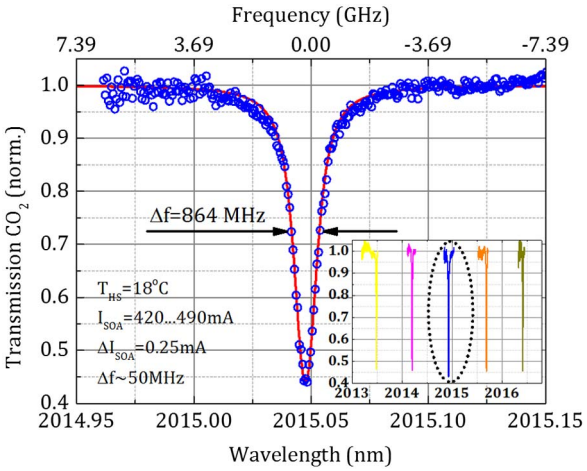

Fig. 7. Absorption line of CO_2 measured (blue circles) with the AMZI integrated tunable laser source and overlapped with the absorption profile simulated (solid red line) with the HITRAN software using parameters of the reference gas cell used for the experiment. The inset presents the measured absorption spectra of four more CO_2 transitions.

4. CONCLUSIONS

A long wavelength laser realized as a PIC operating in the wavelength range beyond 2 μm has been presented. The PIC including four such tunable lasers was fabricated on a shared wafer basis as a standard cell within a MPW run fabricated using long wavelength active-passive integration technology on indium phosphide. The process flow is nearly identical to that of the 1.5 μm COBRA active-passive integration technology. The laser provided a single longitudinal-mode output over a record tuning range of 31 nm centered at 2027 nm. The wavelength tuning mechanism based on the reverse biased ERMs allowed the targeting of an absorption line of carbon dioxide. The measurement of the absorption profile was possible by fine tuning the laser without mode hops using a single control signal, the current injection into the SOA section. This experiment demonstrates the feasibility of such a laser design for use in gas spectroscopy systems. The wide tuning range makes a single device sufficiently versatile to address various types of gas species. Furthermore, integration of an array of such individually controlled lasers and possibility of co-integration of other functionalities enables a simultaneous analysis of a gas mixture with a single monolithic chip.

Funding. Stichting voor de Technische Wetenschappen (STW) (11360-LWAVETECH); Agentschap NL (IOP Photonic Devices IPD100025-TULGAS); European Union Seventh Framework Programme (FP7) (257210-PARADIGM).

REFERENCES

1. M. Smit, X. Leijtens, H. Ambrosius, E. Bente, J. van der Tol, B. Smalbrugge, T. de Vries, E.-J. Geluk, J. Bolk, R. van Veldhoven, L. Augustin, P. Thijs, D. D'Agostino, H. Rabbani, K. Lawniczuk, S. Stopinski, S. Tahvili, A. Corradi, E. Kleijn, D. Dzibrou, M. Felicetti, E. Bitincka, V. Moskalenko, J. Zhao, R. Santos, G. Gilardi, W. Yao, K. Williams, P. Stabile, P. Kuindersma, J. Pello, S. Bhat, Y. Jiao, D. Heiss, G. Roelkens, M. Wale, P. Firth, F. Soares, N. Grote, M. Schell, H. Debregeas, M. Achouche, J.-L. Gentner, A. Bakker, T. Korthorst, D. Gallagher, A. Dabbs, A. Melloni, F. Morichetti, D. Melati, A. Wonfor, R. Penty, R. Broeke, B. Musk, and D. Robbins, "An introduction to InP-based generic integration technology," Semicond. Sci. Technol. **29**, 83001–83041 (2014).
2. J. G. Crowder, S. D. Smith, A. Vass, and J. Keddie, "Infrared methods for gas detection," in *Mid-Infrared Semiconductor Optoelectronics*, A. Krier, ed. (Springer, 2006) Vol. **118**, pp. 595–613.
3. Y. Ikeda, G. M. Choi, D. H. Chung, K. Fukuzato, and T. Nakajima, "Sensor development of CO_2 gas temperature and concentration using 2 μm DFB semiconductor laser," in *10th International Symposium on Applications of Laser Techniques to Fluid Mechanics* (2000), pp. 483–496.
4. G. Roelkens, U. Dave, A. Gassenq, N. Hattasan, C. Hu, B. Kuyken, F. Leo, A. Malik, M. Muneeb, E. Ryckeboer, D. Sanchez, S. Uvin, R. Wang, Z. Hens, R. Baets, Y. Shimura, F. Gencarelli, B. Vincent, R. Loo, J. Van Campenhout, L. Cerutti, J.-B. Rodriguez, E. Tournie, X. Chen, M. Nedeljkovic, G. Mashanovich, L. Shen, N. Healy, A. C. Peacock, X. Liu, R. Osgood, and W. M. J. Green, "Silicon-based photonic integration beyond the telecommunication wavelength range," IEEE J. Sel. Top. Quantum Electron. **20**, 394–404 (2014).
5. T. Hosoda, T. Feng, L. Shterengas, G. Kipshidze, and G. Belenky, "High power cascade diode lasers emitting near 2 μm," Appl. Phys. Lett. **108**, 131109 (2016).
6. S. Forouhar, R. M. Briggs, C. Frez, K. J. Franz, and A. Ksendzov, "High-power laterally coupled distributed-feedback GaSb-based diode lasers at 2 μm wavelength," Appl. Phys. Lett. **100**, 031107 (2012).
7. L. Shterengas, G. Kipshidze, T. Hosoda, M. Wang, T. Feng, and G. Belenky, "Cascade type-I quantum well GaSb-based diode lasers," Photonics **3**, 27 (2016).
8. Y. Gu, Y. Zhang, Y. Cao, L. Zhou, X. Chen, H. Li, and S. Xi, "2.4 μm InP-based antimony-free triangular quantum well lasers in continuous-wave operation above room temperature," Appl. Phys. Express **7**, 032701 (2014).
9. Y. Y. Cao, Y. G. Zhang, Y. Gu, X. Y. Chen, L. Zhou, and H. Li, "2.7 μm InAs quantum well lasers on InP-based InAlAs metamorphic buffer layers," Appl. Phys. Lett. **102**, 201111 (2013).
10. S. Sprengel, C. Grasse, P. Wiecha, A. Andrejew, T. Gruendl, G. Boehm, R. Meyer, and M. C. Amann, "InP-based type-II quantum-well lasers and LEDs," IEEE J. Sel. Top. Quantum Electron. **19**, 1900909 (2013).
11. G. Maisons, C. Gilles, L. Orbe, G. Carpintero, J. Abautret, and M. Carras, "Monolithic integration of a widely-tunable mid-infrared source based on DFB QCL array and echelle grating," in *Laser Applications to Chemical, Security and Environmental Analysis 2016*, Heidelberg Germany, 25–28 July 2016 (Optical Society of America, 2016), paper LTh3E.7.
12. A. Spott, J. Peters, M. L. Davenport, E. J. Stanton, C. D. Merritt, W. W. Bewley, I. Vurgaftman, C. S. Kim, J. R. Meyer, J. Kirch, L. J. Mawst, D. Botez, and J. E. Bowers, "Quantum cascade laser on silicon," Optica **3**, 545–551 (2016).
13. J. Dong, A. Ubukata, and K. Matsumoto, "Characteristics dependence on confinement structure and single-mode operation in 2-μm compressively strained InGaAs-InGaAsP quantum-well lasers," IEEE Photonics Technol. Lett. **10**, 513–515 (1998).
14. T. Sato, M. Mitsuhara, T. Watanabe, K. Kasaya, T. Takeshita, and Y. Kondo, "2.1-μm-wavelength InGaAs multiple-Quantum-well distributed feedback lasers grown by MOVPE using Sb surfactant," IEEE J. Sel. Top. Quantum Electron. **13**, 1079–1083 (2007).
15. W. Zeller, M. Legge, A. Somers, W. Kaiser, J. Koeth, and A. Forchel, "Singlemode emission at 2 μm wavelength with InP based quantum dash DFB lasers," Electron. Lett. **44**, 354–356 (2008).
16. B. W. Tilma, Y. Jiao, J. Kotani, B. Smalbrugge, H. P. M. M. Ambrosius, P. J. Thijs, X. J. M. Leijtens, R. Notzel, M. K. Smit, and E. A. J. M. Bente, "Integrated tunable quantum-dot laser for optical coherence tomography in the 1.7 μm wavelength region," IEEE J. Quantum Electron. **48**, 87–98 (2012).
17. S. Latkowski, P. Thijs, P. J. van Veldhoven, H. Rabbani-Haghighi, M. K. Smit, and E. A. J. M. Bente, "Small signal modal gain measurement of ridge waveguide semiconductor optical amplifiers operating at 2 μm suitable for active-passive integration," in *Photonics Conference (IPC)* (IEEE, 2013), pp. 258–259.
18. D. D'Agostino, S. Tahvilli, S. Latkowski, P. J. Veldhoven, H. Rabbani-Haghighi, C. Jin, B. Docter, H. Ambrosius, E. Bente, D. Lenstra, and M. Smit, "Monolithically integrated widely tunable coupled cavity laser source for gas sensing applications around 2.0 μm wavelength," in *Advanced Photonics* (Optical Society of America, 2015), paper JT5A.1.

19. S. Latkowski, D. D'Agostino, P. J. van Veldhoven, H. Rabbani-Haghighi, B. Docter, H. Ambrosius, M. Smit, K. Williams, and E. A. J. M. Bente, "Monolithically integrated tunable laser source operating at 2 μm for gas sensing applications," in *Photonics Conference (IPC)* (IEEE, 2015), pp. 535–536.
20. S. Latkowski and D. Lenstra, "Lasers in InP generic photonic integration technology platforms," Adv. Opt. Technol. **4**, 179–188 (2015).
21. S. Latkowski, M. Smit, and E. A. J. M. Bente, "Integrated tunable semiconductor laser geometry based on asymmetric Mach–Zehnder interferometers for gas sensing applications," in *Proceedings of the 17th Annual Symposium of the IEEE Photonics Society Benelux Chapter* (IEEE, 2012).
22. S. Latkowski, A. Hänsel, N. Bhattacharya, T. de Vries, L. Augustin, K. Williams, M. Smit, and E. Bente, "Novel widely tunable monolithically integrated laser source," IEEE Photonics J. **7**, 1–9 (2015).
23. S. Latkowski, P. J. van Veldhoven, A. Hänsel, D. D'Agostino, H. Rabbani-Haghighi, B. Docter, N. Bhattacharya, P. Thijs, H. Ambrosius, and M. Smit, "Indium phosphide monolithic photonic integrated circuits for gas sensing applications," in *Proceedings of 18th European Conference on Integrated Optics (ECIO)* (2016).
24. S. Hein, A. Somers, W. Kaiser, S. Höfling, J. P. Reithmaier, and A. Forchel, "Singlemode InAs/InP quantum dash distributed feedback lasers emitting in 1.9 μm range," Electron. Lett. **44**, 527–528 (2008).
25. T. Kanai, N. Fujiwara, Y. Ohiso, H. Ishii, M. Shimokozono, and M. Itoh, "2-μm wavelength tunable distributed Bragg reflector laser," IEICE Electron. Exp. **13**, 20160655 (2016).
26. A. Spott, M. Davenport, J. Peters, J. Bovington, M. J. R. Heck, E. J. Stanton, I. Vurgaftman, J. Meyer, and J. Bowers, "Heterogeneously integrated 2.0 μm CW hybrid silicon lasers at room temperature," Opt. Lett. **40**, 1480–1483 (2015).
27. S. Latkowski, P. J. van Veldhoven, D. D'Agostino, H. Rabbani-Haghighi, B. Docter, P. Thijs, H. Ambrosius, K. Williams, E. Bente, and M. Smit, "COBRA long wavelength active-passive monolithic photonic integration technology platform," in *Proceedings of 18th European Conference on Integrated Optics (ECIO)* (2016).
28. T. Sato, M. Mitsuhara, T. Watanabe, and Y. Kondo, "Surfactant-mediated growth of InGaAs multiple-quantum-well lasers emitting at 2.1 μm by metalorganic vapor phase epitaxy," Appl. Phys. Lett. **87**, 211903 (2005).
29. J. D. Thomson, H. D. Summers, P. J. Hulyer, P. M. Smowton, and P. Blood, "Determination of single-pass optical gain and internal loss using a multisection device," Appl. Phys. Lett. **75**, 2527–2529 (1999).
30. L. A. Coldren, S. W. Corzine, and M. L. Mashanovitch, *Diode Lasers and Photonic Integrated Circuits* (Wiley, 2012), Chapter 3.
31. S. Latkowski, A. Hänsel, N. Bhattacharya, T. de Vries, L. Augustin, K. Williams, M. Smit, and E. Bente, "Monolithically integrated array of widely tunable laser sources for multispecies gas sensing applications," in *OSA Technical Digest, Optical Fiber Communication Conference* (Optical Society of America, 2016), paper W4H.2.
32. "HITRAN," https://www.cfa.harvard.edu/hitran/.
33. "HITRAN on the Web," http://hitran.iao.ru/.